

EC PROJECT  
EVG1-CT-2002-00069



REL. I. E. F.



*RELIable Information on Earthquake Faulting*

Large Earthquake Faulting and Implications for the Seismic  
Hazard Assessment in Europe:  
*The Izmit-Duzce earthquake sequence of August-November 1999*  
*(Turkey, Mw 7.4, 7.1)*

# Maps of seismic hazard scenarios

*Deliverable no. 25*  
*January 2006*

WP 6: Integration of multidisciplinary data for seismic hazard assessment

WP 9: Multidisciplinary seismic hazard assessment

Prepared by K. Atakan, M. B. Sørensen (UiB)  
and P.M. Mai, G. Hillers (ETHZ)

*PARTNER 6: Department of Earth Science, University of Bergen*  
*PARTNER 4: Institute of Geophysics, ETH Zurich (Switzerland)*



## **List of Contents**

Summary

1. Introduction

2. Hybrid ground motion simulations based on complex source models

2.1. Tectonic setting

2.2. Ground motion simulation methodology

2.3. Input scenarios

2.4. Simulation results

3. Scenario earthquakes and ground motions from multi-cycle earthquake simulations

3.1. Background

3.2. Catalog of simulated events

3.3. Pseudo-dynamic rupture models

3.4. Ground motion simulation and seismic shaking maps

4. Synthesis and concluding remarks

Acknowledgements

References

Appendix I: Revision of the long-term seismicity in the greater Marmara Region by N.N. Ambraseys (Sub-contractor's report)

## Summary

Within the framework of workpackage 6 (WP06) of the RELIEF project, multidisciplinary datasets are integrated for seismic hazard assessment. The different approaches used in assessing the seismic hazard all require different data sets. The input data sets were outlined previously for the probabilistic methods including both the poissonian and time-dependant recurrence models. In the present report, input data for the deterministic computations are explained. Results from ground motion simulations are then presented as seismic hazard scenarios. These deterministic calculations are performed as a part of workpackage 9 (WP09), using two different methods. The first method applied is a hybrid ground motion simulation technique including a multi-asperity, complex source model as an input, and is conducted by Partner 6 (University of Bergen - UiB). The second method involves ground motion calculations based on multi-cycle earthquake simulations and is conducted by Partner 4 (ETH, Zurich). The results are presented in terms of various maps showing the ground motion distribution in Istanbul and the surrounding areas. The simulation results are also compared to the previously obtained probabilistic seismic hazard results.

### 1. Introduction

The city of Istanbul is subject to a significant seismic hazard due to its close proximity to the Marmara Sea segment of the North Anatolian Fault (NAF) (Figure 1.1). During the last century there has been a westward migration of large, destructive earthquakes along the NAF with the latest events occurring in Izmit and Duzce in 1999 (e.g. Barka et al., 1999). Following these large earthquakes, there has been an increase in the coulomb stress along the Marmara Sea segment (Hubert-Ferrari et al., 2000) which, together with the fact that no large earthquakes have occurred at least since 1766 (Barka et al., 2002), indicates that a large earthquake is likely to break this part of the NAF within the life time of the present city environment (Parsons et al., 2000; Parsons, 2004).

Seismic hazard in Istanbul has previously been estimated using probabilistic methods (Atakan et al., 2002; Erdik et al., 2004). Within the framework of the RELIEF Project, revised probabilistic seismic hazard assessment for Istanbul and the surrounding areas was completed. These results were presented in earlier reports (see RELIEF Deliverable 18). For future risk mitigation and city planning, a reliable estimate of the seismic hazard in Istanbul is needed. Recently, increased knowledge on the NAF within the Marmara Sea allowed other methods to be applied in the hazard

assessment. Pulido et al. (2004) modeled the bedrock ground motions due to a finite extent scenario earthquake source ( $M=7.5$ ) in the Marmara Sea using a hybrid broadband simulation technique, and hereby gave a first insight to the complexity of ground shaking to be expected in a future earthquake. Such results are important due to their direct engineering implications. In the present report, we present the results from two separate studies on ground motion simulations. The first one of these is conducted by Partner 6 (UiB, Bergen) and deals with ground motion simulations using hybrid ground motion simulations based on complex source models as described in Pulido et al. (2004). The second method involves ground motion calculations based on multi-cycle earthquake simulations and is conducted by Partner 4 (ETH, Zurich). The results are presented in terms of various maps showing the ground motion distribution in Istanbul and the surrounding areas. The simulation results are also compared to the previously obtained probabilistic seismic hazard results.

## **2. Hybrid ground motion simulations based on complex source models**

This section is written by M.B. Sørensen and K. Atakan, Department of Earth Science, University of Bergen

Simulations are based on a multiasperity source model that involves the combined rupture of the North Anatolian Fault (NAF) segments beneath the Marmara Sea. A hybrid model is adopted combining a deterministic simulation of the low frequencies (0.1-1.0 Hz) with a semi-stochastic simulation of the high frequencies (1.0-10.0 Hz) using empirical Green's functions. In the following, we describe the details of the methodology and the input scenario, and discuss the resulting simulated ground motion distribution in Istanbul and the surrounding areas.

### **2.1. Tectonic setting**

The NAF is a ca 1200 km long fault structure extending through the northern part of Turkey from Erzincan in the East to the Aegean Sea in the West. The structure forms the boundary between the westward moving Anatolian Block with respect to the Eurasian plate, accommodating the relative motion through right-lateral strike-slip motion. In the westernmost part, around the Marmara Sea, the NAF splits into two main branches (Figure 1.1). Studying GPS displacement vectors, Okay et al. (2000) showed that the main strain accumulation takes place along the northernmost fault branch, which is therefore the target of our ground motion modeling. This northernmost fault branch consists of two main segments, namely the Central Marmara Fault (CMF) and the North

Boundary Fault (NBF). The CMF has a strike almost parallel to the general stress orientation in the region and is therefore expected to break in a pure strike-slip earthquake. The NBF, on the other hand, is oblique to the stress orientation and constitutes a releasing bend on the NAF. We therefore expect an oblique normal mechanism along this segment. The velocity of the regional plate motion is approximately 2 cm/yr (Straub et al., 1997). Major historic earthquakes along these segments of the NAF include the 1509 earthquake (M=7.2) and the 1766 earthquake sequence (M=7.1 and M=7.4). In addition, a M=6.4 earthquake has ruptured along the NBF in 1963 (Ambraseys and Jackson, 2000).

## **2.2. Ground motion simulation methodology**

In the present study we have followed the approach of Pulido and Kubo (2004) and Pulido et al. (2004), using a hybrid method for modeling the ground motion. This procedure combines a deterministic simulation at low frequencies (0.1-1 Hz) with a semi-stochastic simulation at high frequencies (1-10 Hz). A finite-extent scenario earthquake source embedded in a flat-layered 1D velocity structure is assumed. The source consists of a number of asperities, which are divided into subfaults assumed to be point sources. The total ground motion at a given site is obtained by summing the contributions from the different subfaults. For the low frequencies, subfault contributions are calculated using discrete wave number theory (Bouchon, 1981) and summed assuming a given rupture velocity. At high frequencies, the subfault contributions are calculated using the stochastic method of Boore (1983) and summed using the empirical Greens function method of Irikura (1986). The radiation pattern is changed from a theoretical double-couple radiation pattern at low frequencies to a uniform radiation pattern at high frequencies following Pulido and Kubo (2004).

The ground motion simulations are performed at bedrock level and therefore do not take local site effects into account. This is important to keep in mind when interpreting the simulation results since local site effects are indeed present and important, especially in the southwestern part of the city (e.g. Birgören et al., 2004; Sørensen et al., in review). This issue is being addressed by Sørensen et al. (in review), aiming to combine ground motion simulation results with information about local site effects.

As input for the modelling, the earthquake source scenario needs to be defined in terms of the location, geometry and the asperities of the rupturing fault together with asperity parameters such

as rise time, rupture velocity, stress drop and seismic moment. In addition, the properties of the surrounding crust need to be defined giving velocity structure and attenuation characteristics.

### **2.3. Input scenarios**

In the following, we describe the “standard scenario” input, which will later be used for comparison to other scenarios (see RELIEF-Deliverable 26). The location and dimensions of the rupturing fault are defined by considering the local tectonics and seismicity. We assume a combined rupture of the CMF and NBF segments of the NAF. A total fault length of 130 km is used, which is confined to the area between the 1999 Izmit rupture to the east and the 1912 Ganos rupture to the west (Figure 1.1). We assume a fault width of 20 km in agreement with the depth of the seismogenic zone as indicated by the depth distribution of seismicity (Gurbuz et al., 2000). The fault plane solution used is the one of Pulido et al. (2004) with pure right-lateral strike-slip faulting along the CMF and an oblique-normal mechanism along the NBF. Two asperities are defined covering 22% of the fault plane following the empirical results of Somerville et al. (1999). These are located near the intersection of the CMF and NBF segments (Figure 1.1). This area has previously been suggested to be a seismic gap (Gurbuz et al., 2000), characterized by its low seismicity. The seismic moment released by the scenario earthquake is  $2.0 \times 10^{20}$  Nm, which is an average value of the seismic moments estimated by different authors for the 1999 Izmit earthquake (Pulido et al., 2004). The velocity model used in the modelling is the one used for routine location of earthquakes in the region (Figure 2.1). For the cut-off frequency  $f_{\max}$  we use a value of 10 Hz, which is also the upper frequency limit of the calculations. In practice this implies that the high-frequency decay of the ground motion is mainly controlled by attenuation.

For the standard scenario, the rupture initiation point is located at the westernmost edge of asperity 1 (Figure 1.1). This is believed to be a likely location since the boarder regions of asperities represent significant changes in physical properties of the fault and thereby zones of weakness. Based on seismic moment, fault area and asperity area, the stress drop is calculated based on the relations of Das and Kostrov (1986) and Brune (1970) following Pulido et al. (2004). Rupture velocity and rise time are taken from Pulido et al. (2004) for the standard scenario. The regional attenuation is defined in terms of Q. For the standard scenario we have used the “Low Attenuation Model” of Pulido et al. (2004). The source parameters of the standard scenario are summarized in Table 1. It should be noted that this scenario is considered as a conservative approximation.

## 2.4. Simulation results

The simulated PGA and PGV values for the standard scenario are shown in Figure 2.2. The largest accelerations are predicted in the southernmost part of the city, which is also located closest to the rupturing fault. Here we can expect bedrock accelerations of 0.5g or more in some places. There is a very strong forward directivity effect on the ground motions, which is especially evident in the PGV distribution. Largest velocities are expected in the southeastern part of the city, where we predict velocities up to 125 cm/s. Due to the forward directivity, the shaking is extended far towards East from the rupturing fault. This may have important implications along the populated areas around the Izmit gulf.

## 3. Scenario earthquakes and ground motions from multi-cycle earthquake simulations

This section is written by P. Martin Mai and G. Hillers of the Institute of Geophysics, ETH Hoenggerberg, Zürich, Switzerland.

### 3.1 Background

One of the most fundamental questions in earthquake physics is related to the origin and persistence of earthquake complexity, and how such rupture heterogeneity affects near-source ground motion estimation. It is of particular interest to assess not only the expected level of ground motion at a given site, but also the variability of ground motion intensity measures (e.g. *PGA*, *PGV*, or spectral acceleration  $S_A$  at a set of periods). Since the distributions of recorded ground motions in terms of source-site distance and magnitudes are limited in that very few data exist in the very near-source range for large earthquakes, physically realistic, broadband simulations of ground motions play an increasingly important role in seismic hazard studies.

As described in RELIEF Deliverable 24 and a number of submitted/accepted papers, we have developed a three-dimensional elastic continuous fault model governed by rate- and state-dependent friction (*Hillers and Miller, 2005 a, b; Hillers et al, 2005 a, b*) for multi-cycle earthquake simulations with realistic variations in the frictional properties across the fault. The spatial variability of the governing friction-model parameter, the critical slip distance  $L$ , serves as a proxy

to capture various degrees of fault maturity or geometrical fault irregularities. With our chosen model setup and friction parameterization (see RELIEF Deliverable 24 for details), we are able to generate a wide range of earthquake phenomena (in terms of frequency size statistics and the temporal occurrence of earthquakes) as well as slip distributions that closely resemble slip maps of past earthquakes (in terms of spatial variability of slip and the rupture nucleation point). In this Deliverable 25, we show example calculations of ground-motions in the Istanbul area using our multi-cycle simulations, combined with the pseudo-dynamic source characterization by *Mai* (2001) and *Guatteri et al.* (2003, 2004). This demonstrates the feasibility of this truly innovative method for ground motion prediction and seismic hazard studies.

### 3.2 Catalog of simulated events

Figure 3.1 shows some statistics of the catalog of scenario earthquakes that we were able to compile from our multi-cycle simulations, considering a number of runs with different fault sizes and friction-parameters realizations. Here we only show those events that are, in general, relevant for near-source ground motions, starting at  $M_w \sim 5.5$  events. The largest events are about  $M_w = 7.5$ . Figure 4.6 in RELIEF Deliverable 24 displays individual slip distributions, along with the rupture nucleation points, of a compilation of selected events, showing the degree of slip variation on the fault. Since these models agree well with observed slip and rupture-nucleation patterns of past earthquakes (*Mai and Beroza*, 2000, 2002; *Mai et al.*, 2005), we utilize our simulated slip-model catalog for generating source rupture models for ground motion calculations.

### 3.3 Pseudo-dynamic rupture models

In order to generate source-rupture models that are appropriate for ground motion calculations from our catalog of simulated slip maps, we have to apply certain transformations. First of all, although the spatial distributions of slip are realistic, the maximum displacements on the fault are not. Due to radiation damping in the quasi-dynamic multi-cycle calculations, slip values are too small. We compensate that by re-scaling the slip distributions based on an empirical scaling relation on maximum slip and standard deviation of slip derived from the finite-source database of past earthquakes (see also RELIEF Deliverables 14 and 21). Figure 3.2 illustrates this procedure, showing the finite-source data and the obtained scaling for ~90 imaged rupture models, and how the application of this scaling changes the final slip pattern of the scenario event. This transformation leaves the location and relative size of high-slip regions (asperities) unchanged, but merely creates slightly larger “inter-asperity” distances and realistic values of maximum displacement.

The final step in generating realistic scenario earthquakes involves a physically self-consistent characterization of the temporal rupture evolution (Figure 3.3). We use the pseudo-dynamic source model by *Mai* (2001) and *Guatteri et al* (2003, 2004) for this purpose, which ensures that rupture velocity and rise time are compatible with the underlying static stress change distribution. The rupture-time contours (plotted as thin white lines in Figure 3.3) therefore display some variation (i.e. rupture slowing down or speeding up) depending on the local stresses, likewise the rise time distributions (not shown) exhibit spatial variations reflecting the distance from the fault-plane boundaries and the distance the rupture has traveled along the fault.

Taken together, the slip maps from multi-cycle earthquake simulations, combined with the pseudo-dynamic rupture characterization provides an extremely powerful and efficient approach to generate a large set of physically constrained scenario earthquakes that cover a possibly wide range of magnitudes. Such suites of scenario earthquakes are useful for seismic hazard estimation and the calculation of ground-motions for engineering purposes.

### **3.4 Ground-motion simulation & seismic-shaking maps**

We apply our source-model simulation methodology to ground-motion computations in the Marmara Region, targeting specifically the city of Istanbul. Figure 3.4 shows our chosen distribution of receivers, where we use only a single large fault (up to 100 km long) for simplicity. This modeling choice also reflects the fact that a large part of the expected shaking will be governed by the east-west-striking segment of the Central Marmara Fault (CMF) which points right towards Istanbul and therefore will exert large directivity effects. The recent work by *Pulido et al* (2004), and the work described in section 2, use similar source-site geometry, but does include the Northern Boundary Fault (NBF), which however plays only a minor role for the ground motion generation in Istanbul.

Figure 3.5 displays spatial distributions of peak-ground velocity (*PGV*) and peak-ground acceleration (*PGA*) for the two horizontal components and the corresponding geometric mean, computed for two scenario events that rupture towards the city of Istanbul. The ground motions are computed using a discrete wave-number/finite-element method with a maximum resolving frequency of 1 Hz and using triangular slip-velocity function with variable width (rise time) according to the pseudo-dynamic modeling. At this point we have not included stochastic high-

frequency wave generation by means of random-vibration theory or wave scattering; such high-frequency contributions will complement this work, but are left for future studies. Because we so far have only computed long-period motions, we do not show comparisons of our simulated motions with empirical ground-motion attenuation models since those contain information from the full broadband nature of the recordings.

Our simulations show very strong directivity effects which increase the shaking level in particular in the western coastal regions of the city of Istanbul. An important aspect of this observation is that these are also the heavily industrialized areas, partly built on soft sediments, for which soil amplification effects are expected. The combination of these source(-directivity) effects with local site effects therefore poses a major seismic hazard.

In this study we demonstrate that multi-cycle earthquake simulations, combined with the pseudo-dynamic source characterization, represent a powerful new tool for physically realistic near-source ground motion simulations. The resulting ground-shaking maps could be further used for probabilistic seismic hazard calculations, whereas time series at individual sites are useful for earthquake engineering purposes. In this pilot study we have not yet carried out these steps which will be left for future work. We have also omitted, for simplicity, stochastic high-frequency simulations, either by means of random-vibration theory or by inclusion of scattering operators, in order to not obscure the basic features of the long-period motions and their directivity effects. High-frequency contributions will decrease the influence of directivity due to incoherent summation of phase arrivals, but of course will strongly affect peak-ground acceleration and spectral acceleration.

#### **4. Concluding remarks**

Previously, RELIEF Partner 6 (UiB) had performed two probabilistic seismic hazard studies in the Marmara region. One study was a continuation of the work presented in Atakan et al. (2002) where three different source models (one poissonian and two renewal models) and four attenuation models were compared. Calculations were performed for the Istanbul area. In this continued work, the area of study was extended to the whole Marmara Sea region, whereas the same catalogue, source models and attenuation models were used. In the other study we applied a different source zonation, a new earthquake catalogue and two of the attenuation models also used by Atakan et al. (2002) (Ambraseys et al. (1996) and Sadigh et al. (1997)), assuming poissonian earthquake occurrence. These two studies were described in detail in previous deliverables (RELIEF-Deliverable 18). Here,

we can mention briefly that the Marmara Sea Region and in particular the city of Istanbul is exposed to a significant earthquake hazard and strong ground shaking. Probabilistic seismic hazard maps for a 10 % probability of exceedence in 50 years show that ground motion levels as high as 0.4g can be expected.

The ground motion simulation techniques applied for estimating the seismic hazard are in general superior to the probabilistic seismic hazard computations, since they involve physically based fault rupture scenarios. The two separate simulation techniques described in this report in previous sections show that the resulting ground motion is significantly more complex than the probabilistic maps. The complex pattern of ground motion distribution reflects the source complexity as well as the path effects as compared to the PGA in PSHA. In the present study the ground motion simulations were performed for bedrock conditions and therefore the possible site effects were not included. However, the effect of the local site conditions was described in a previous report (RELIEF Deliverable 18).

Another aspect which is not mentioned in detail in this report is the variation of the ground motion due to different input scenarios. The influence of critical parameters defining the source complexity are explained in more detail in another report (see RELIEF Deliverable 26). In that report the uncertainties associated with the ground motion simulations are quantified using a parameter sensitivity study. The reader is therefore referred to RELIEF Deliverables 16, 17, 18, 24, 25, 26 and 27 for comprehensive review of the entire work on seismic hazard assessment conducted within the framework of the Project.

### **Acknowledgements**

We appreciate the contributions of the partners of the RELIEF Project, which provide the basis for the seismic hazard analysis presented in this report.

### **References**

Ambraseys, N.N. and Jackson, J.A., (2000): Seismicity of the Sea of Marmara (Turkey) since 1500, *Geophys. J. Int.*, 141, F1-F6.

- Ambraseys, N. N., Simpson, K. A. and Bommer, J. J. (1996): Prediction of horizontal response spectra in Europe, *Earthquake Eng. Struct. Dyn.* 25, 371-400.
- Atakan, K., Ojeda, A., Megraoui, M., Barka, A. A., Erdik, M. And Bodare, A. (2002): Seismic Hazard in Istanbul following the 17 August 1999 Izmit and 12 November 1999 Düzce Earthquakes, *Bulletin of the Seismological Society of America*, 92, 1, 466-482.
- Barka et al., 1999.
- Barka, A., Akyüz, H.S., Altunel, E., Sunal, G., Cakir, Z., Dikbas, A., Yerli, B., Armijo, R., Meyer, B., de Chabaliér, J.B., Rockwell, T., Dolan, J.R., Hartleb, R. Dawson, T., Christofferson, S., Tucker, A., Fumal, T., Langridge, R., Stenner, H., Lettis, W., Bachhuber, J. and Page, W. (2002). The Surface Rupture and Slip Distribution of the 17 August 1999 Izmit Earthquake (M 7.4), North Anatolian Fault, *Bulletin of the Seismological Society of America*, 92, 1, 43-60.
- Birgören, G., Özel, O., Fahjan, Y. and Erdik, M., 2004. Determination of site effects in Istanbul area using a small earthquake record of the dense strong motion network, XXIX General Assembly of the European Seismological Commission, Potsdam, Germany, poster no. 249.
- Boore, D. M. (1983): Stochastic simulation of high frequency ground motions based on seismological models of the radiated spectra, *Bull. Seism. Soc. Am.*, 73, 1865-1894.
- Bouchon, M. (1981): A simple method to calculate Green's functions for elastic layered media, *Bull. Seism. Soc. Am.*, 71, 959-971.
- Brune, J., 1970. Tectonic stress and the spectra of seismic shear waves from earthquakes. *J. Geophys. Res.*, 75, 4997-5009.
- Das, S. and Kostrov, B.V., 1986. Fracture of a single asperity on a finite fault: a model for weak earthquakes? In: Das, S., Boatwright, J., Scholz, C. (Eds.). *Earthquake source mechanism*. American Geophysical Union, Washington, pp.91-96.
- Erdik, M., Alpay Biro, Y., Onur, T., Sesetyan, K. and Birgören, G. (1999): Assessment of earthquake hazard in Turkey and neighbouring regions. *Annali di Geofisica*, Vol.42, N0.6, 1125-1138.
- Erdik, M., Demircioglu, M., Sesetyan, K., Durukal, E. And Siyahi, B., 2004. Earthquake hazard in Marmara Region, Turkey, *Soil Dynamics and Earthquake Engineering*, 24, 605-631.
- Guatteri, M., P. M. Mai, et al. (2003). "Strong ground-motion prediction from stochastic-dynamic source models." *Bull. Seis. Soc. Am* **93**(1): 301-313.
- Guatteri, M., P. M. Mai, et al. (2004). "A Pseudo-Dynamic Approximation to Dynamic rupture Models for Strong Ground Motion Prediction." *Bull. Seis. Soc. Am.* **Vol. 94**(No.6): 2051–2063.
- Gurbuz, C., Aktar, M., Eyidogan, H., Cisternas, A., Haessler, H., Barka, A., Ergin, M., Turkelli, N., Polat, O., Ucer, S.B., Kuleli, S., Baris, S., Kaypak, B., Bekler, T., Zor, E., Bicmen, F., and Yoruk, A., 2000. The seismotectonics of the Marmara region (Turkey): results from a microseismic experiment. *Tectonophysics*, 316, 1-17.
- Hillers, G. (2005). On the origin of earthquake complexity on continuum fault models with rate and state

friction, *dissertation presented to the Department of Earth Sciences, ETH Zurich, in partial fulfilment of the doctoral degree (PhD), Dec 20, 2005.*

- Hillers, G., Y. Ben-Zion, and P.M. Mai (2005). Seismicity on a fault controlled by rate-and-state dependent friction with spatial variation of the critical slip distance, *accepted J. Geophys. Res.*, doi:10.1029/2005JB003859R.
- Hillers, G., and S. Miller (2005). Stability regimes of a dilatant, fluid infiltrated fault plane in a 3-D elastic solid, submitted to *J. Geophys. Res.*, *paper number* 2005JB003872.
- Hillers, G., and S. Miller (2005). Dilatancy controlled spatio-temporal slip evolution of a sealed fault with variations of the pore pressure, submitted to *Geophys J. Int.*, *paper number* GJI-2005-0499.
- Hillers, G., P.M. Mai, Y. Ben-Zion, and J.-P. Ampuero (2005). Statistical properties of seismicity of fault zones at different evolutionary stages, *to be submitted to J. Geophys. Res.*
- Hubert-Ferrari, A., Barka, A., Jacques, E., Nalbant, S.S., Meyer, B., Armijo, R., Tapponnier, P. and King, G.C.P. (2000). Seismic hazard in the Marmara Sea region following the 17 August 1999 Izmit earthquake, *Nature*, 404, 269-273.
- Irikura, K. (1986): Prediction of strong acceleration motion using empirical Green's function, *Proceedings of the 7th Japan. Earthq. Eng. Symp.*, 151-156.
- Mai, P. M. (2001). Characterizing earthquake source complexity for improved strong motion prediction. Department of Geophysics. Stanford, Stanford University: 166.
- Mai, P.M., and G.C. Beroza, Source-scaling properties from finite-fault rupture models, *Bull. Seis. Soc. Am.*, Vol. 90, pp. 604-615., 2000.
- Mai, P.M., and G.C. Beroza, A spatial random field model to characterize complexity in earthquake slip, *J. Geophys. Res.*, 107 (B11), art. no.-2308, 2002.
- Mai, P.M., P. Spudich and J. Boatwright, Hypocenter locations in finite-source rupture models, *Bull. Seis. Soc. Am.*, 95(3), 965-98, 2005.
- Okay, A.I., Kaslilar-Özcan, A., Imren, C., Boztepe-Güney, A., Demirbag, E. and Kuscu, I., 2000. Active faults and evolving strike-slip basins in the Marmara Sea, northwest Turkey: a multichannel seismic reflection study, *Tectonophysics*, 321, 189-218.
- Parsons, T., Toda, S., Stein, R.S., Barka, A. and Dietrichs, J.H., 2000. Heightened Odds of Large Earthquakes Near Istanbul: An interaction-Based Probability Calculation, *Science*, 288, 661-665.
- Parsons, T., 2004. Recalculated probability of  $M \geq 7$  earthquakes beneath the Sea of Marmara, Turkey, *Journal of Geophysical Research*, 109, B05304, doi: 10.1029/2003JB002667.
- Pulido, N. and Kubo, T. (2004): Near-fault strong motion complexity of the 2000 Tottori earthquake (Japan) from a broadband source asperity model, *Tectonophysics*, 390, 177-192.
- Pulido, N., A. Ojeda, and K. Atakan (2004). "Strong ground motion estimation in the Sea of Marmara region (Turkey) based on a scenario earthquake." *Tectonophysics* **391**: 357– 374.

- Sadigh, K., Chang, C.-Y., Egan, J. A., Makdisi, F. and Youngs, R. R. (1997): Attenuation relationship for shallow crustal earthquakes based on California strong motion data. *Seismological Research Letters*, 68, 1, 180-189.
- Somerville, P., Irikura, K., Graves, R., Sawada, S., Wald, D., Abrahamson, N., Iwasaki, Y., Kagawa, T., Smith, N., and Kowada, A., 1999. Characterizing crustal earthquake slip models for the prediction of strong ground motion. *Seismol. Res. Lett.*, 70, 59-80.
- Straub, C., Kahle, H.-G., Schindler, C., 1997. GPS and geologic estimates of the tectonic activity in the Marmara region, NW Anatolia. *J. Geophys. Res.* 102, 27 587–27 601.
- Sørensen, M.B., Oprsal, I., Bonnefoy-Claudet, S., Atakan, K., Mai, P.M., Pulido. N. and Yalciner, C. (2005). Local site effects in Ataköy, Istanbul, Turkey, due to a future large earthquake in the Marmara Sea, submitted to *Geophysical Journal International*, June 2005.

**Table 1:** Source parameters for the standard scenario.

Seismic moment	$M_0 = 2.0 \cdot 10^{20}$ Nm
Strike / Dip / Slip, CMF	81.5 / 90 / 180
Strike / Dip / Slip, NBF	110 / 90 / -135
Average stress drop	5.0 MPa
Asperity stress drop	10 MPa
Rise time	3.0 s
Rupture velocity	3.0 km/s
$f_{\max}$	10 Hz
Q	$100 \cdot f^{1.5}$

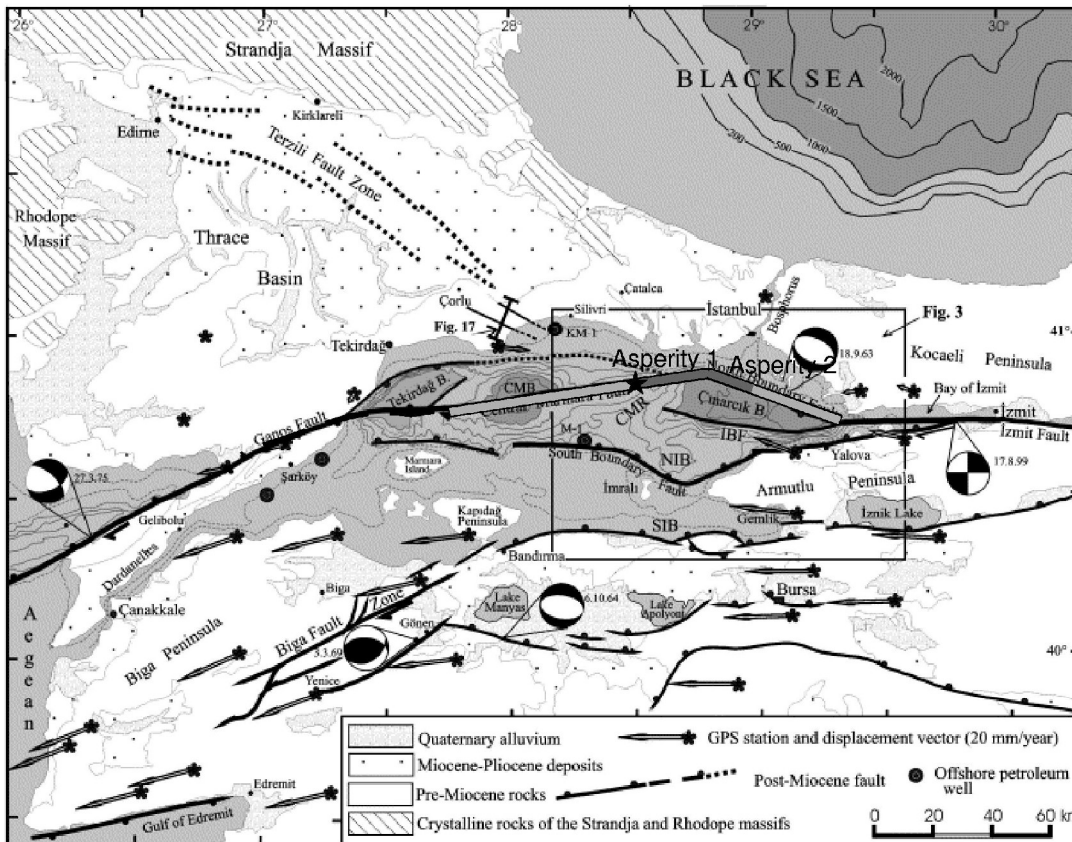


**Figure 1.1.** Map of active faulting in the Marmara Sea region (modified after Okay et al., 2000). The geometry of the standard scenario is given in the central Marmara Sea. The fault rupture is shown as a thick gray line, asperities are shown as darker gray line segments. The star shows the rupture initiation point.



Deliverable no. 25 (Partners # 6 and 4: UiB and ETHZ)



Project No: EVG1-CT-2002-00069

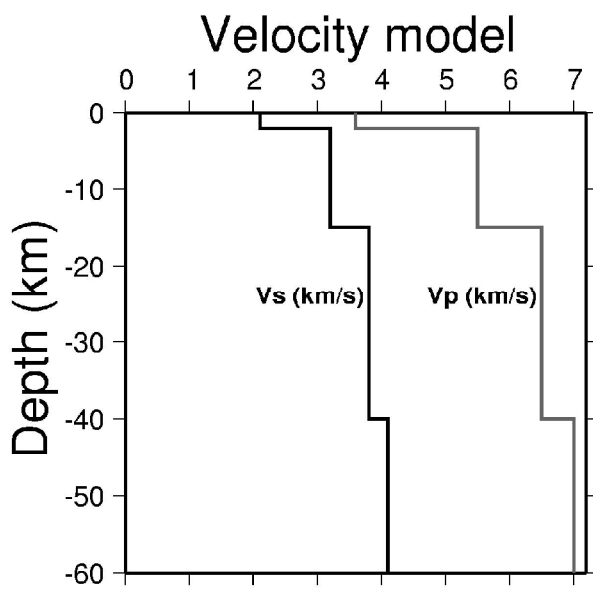


**Figure 2.1.** Velocity model for the Marmara Sea region (Serif Baris, personal communication, 2003).

**Deliverable no. 25 (Partners # 6 and 4: UiB and ETHZ)**



**Project No: EVG1-CT-2002-00069**

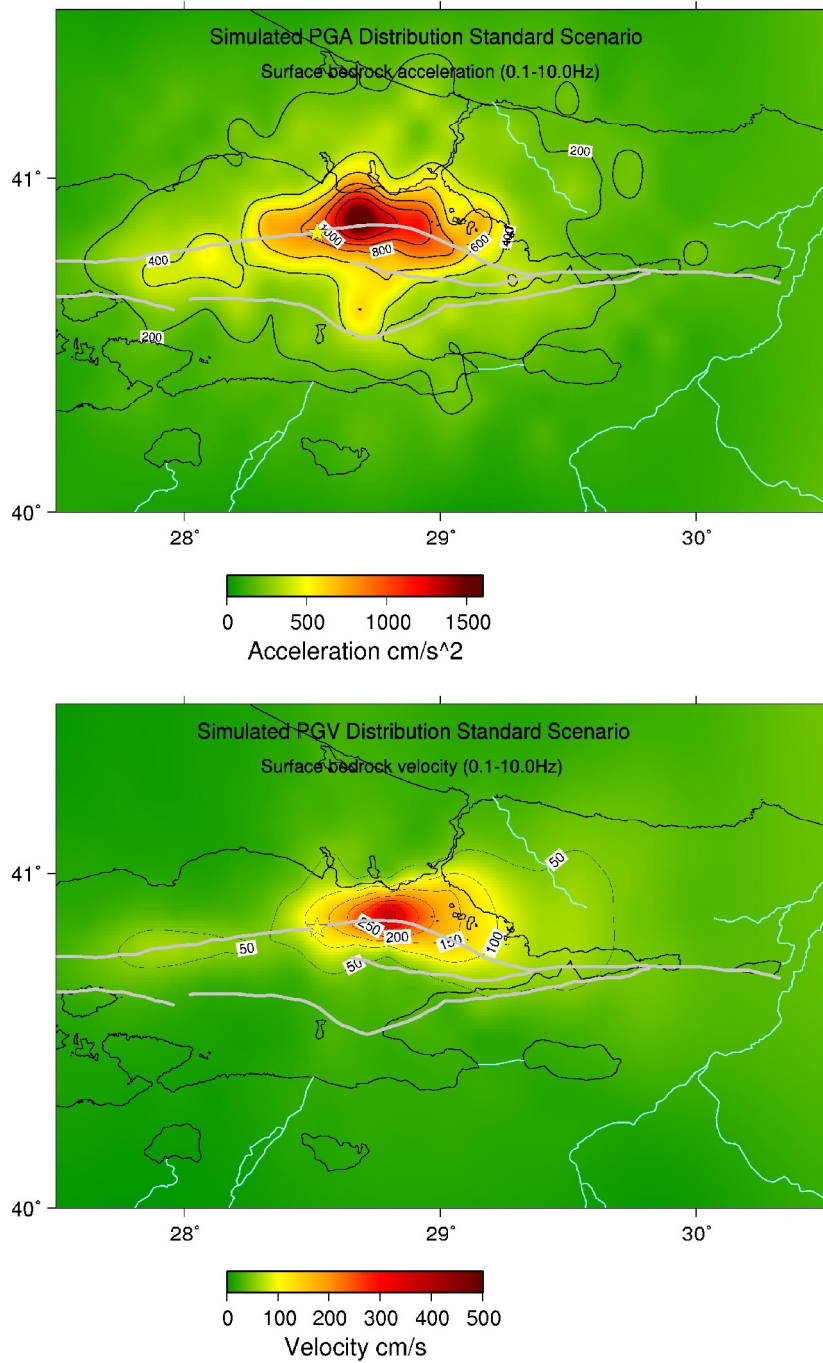


**Figure 2.2.** Simulation result for the “standard scenario”. (top) PGA distribution; (bottom) PGV distribution. Major faults are shown as grey lines and the rupture initiation point as a star.



Deliverable no. 25 (Partners # 6 and 4: UiB and ETHZ)



Project No: EVG1-CT-2002-00069

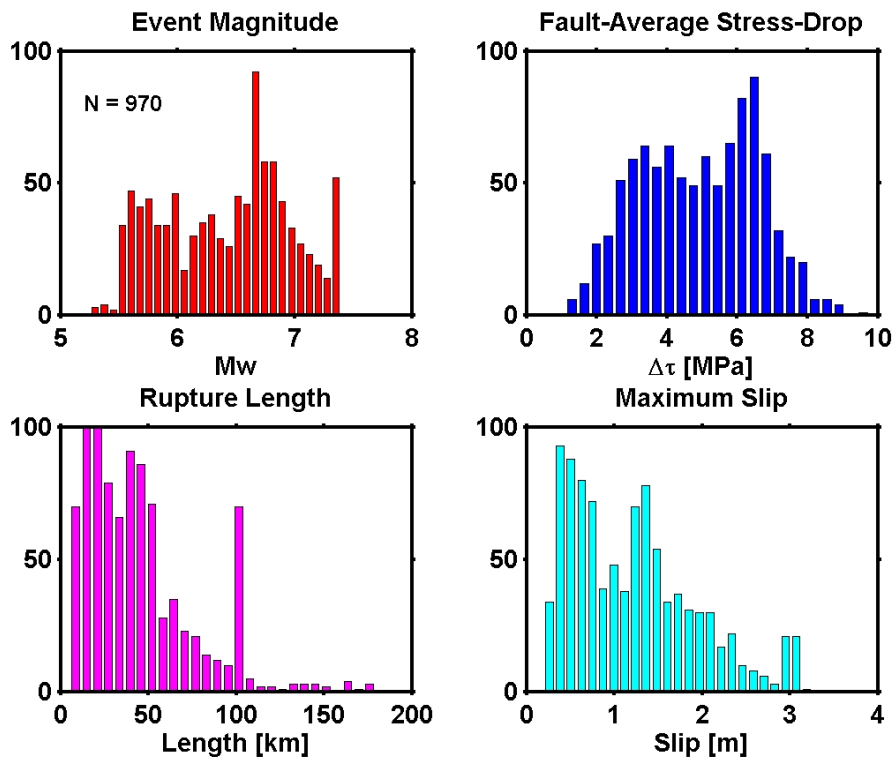


**Figure 3.1** Distributions of source parameters for ~1000 scenario earthquakes, resulting from multi-cycle earthquake simulations with spatially variable frictional properties.

Deliverable no. 25 (Partner # 6 and 4: UiB and ETHZ)



Project No: EVG1-CT-2002-00069

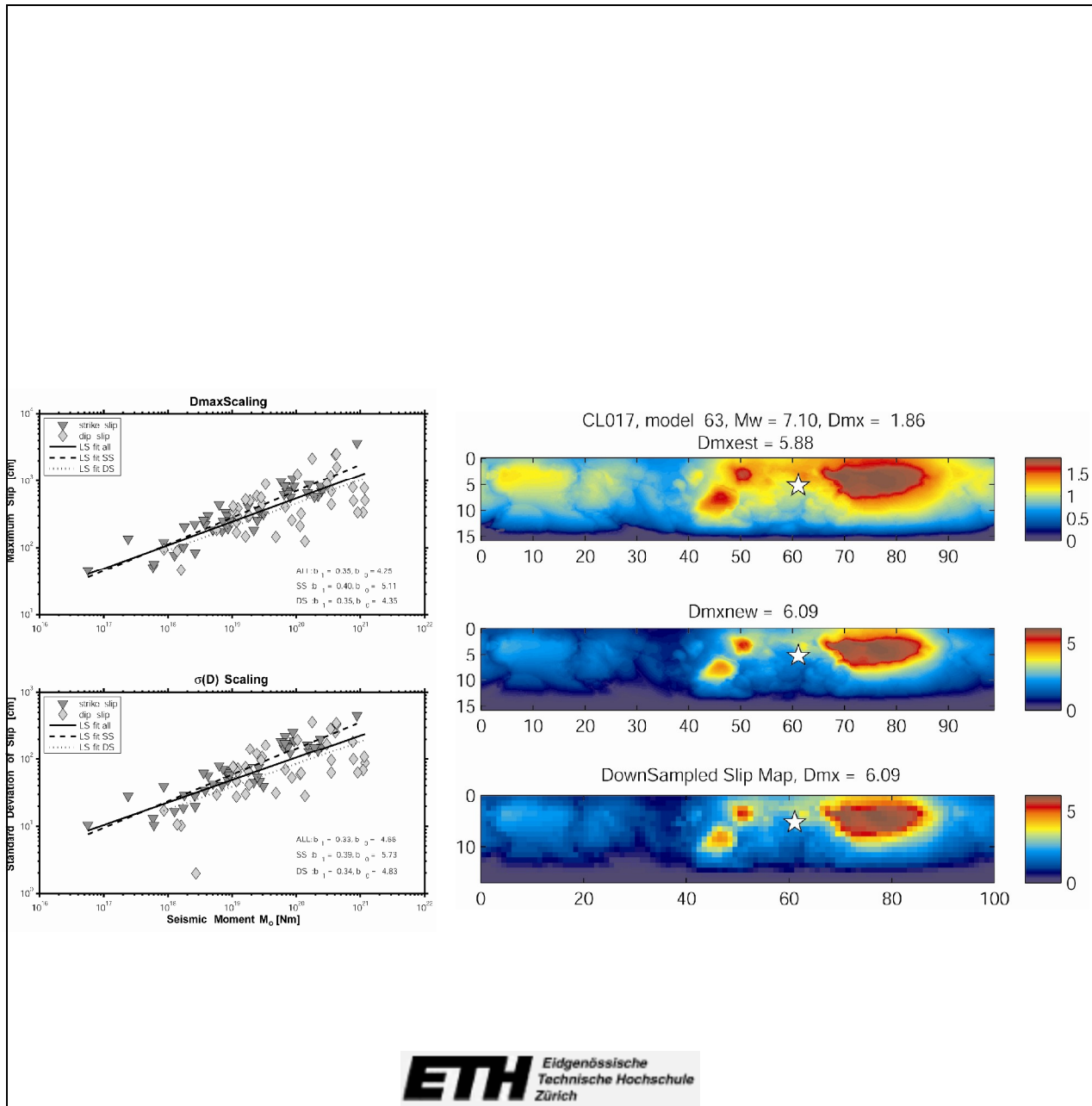


**Figure 3.2** (a – left) Empirical scaling relation for maximum slip (top) and standard deviation of slip (bottom) from source-rupture models in the finite-source database. (b – right) Application of the quadratic slip transformation to an example slip distribution from multi-cycle simulations. The original distribution of slip values (top) is squared such that the transformed slip maps obey to the empirical scaling law (middle). The bottom panel displays the down-sampled (1x1 km grid) slip maps used for ground motion calculations.

Deliverable no. 25 (Partners # 6 and 4: UiB and ETHZ)



Project No: EVG1-CT-2002-00069

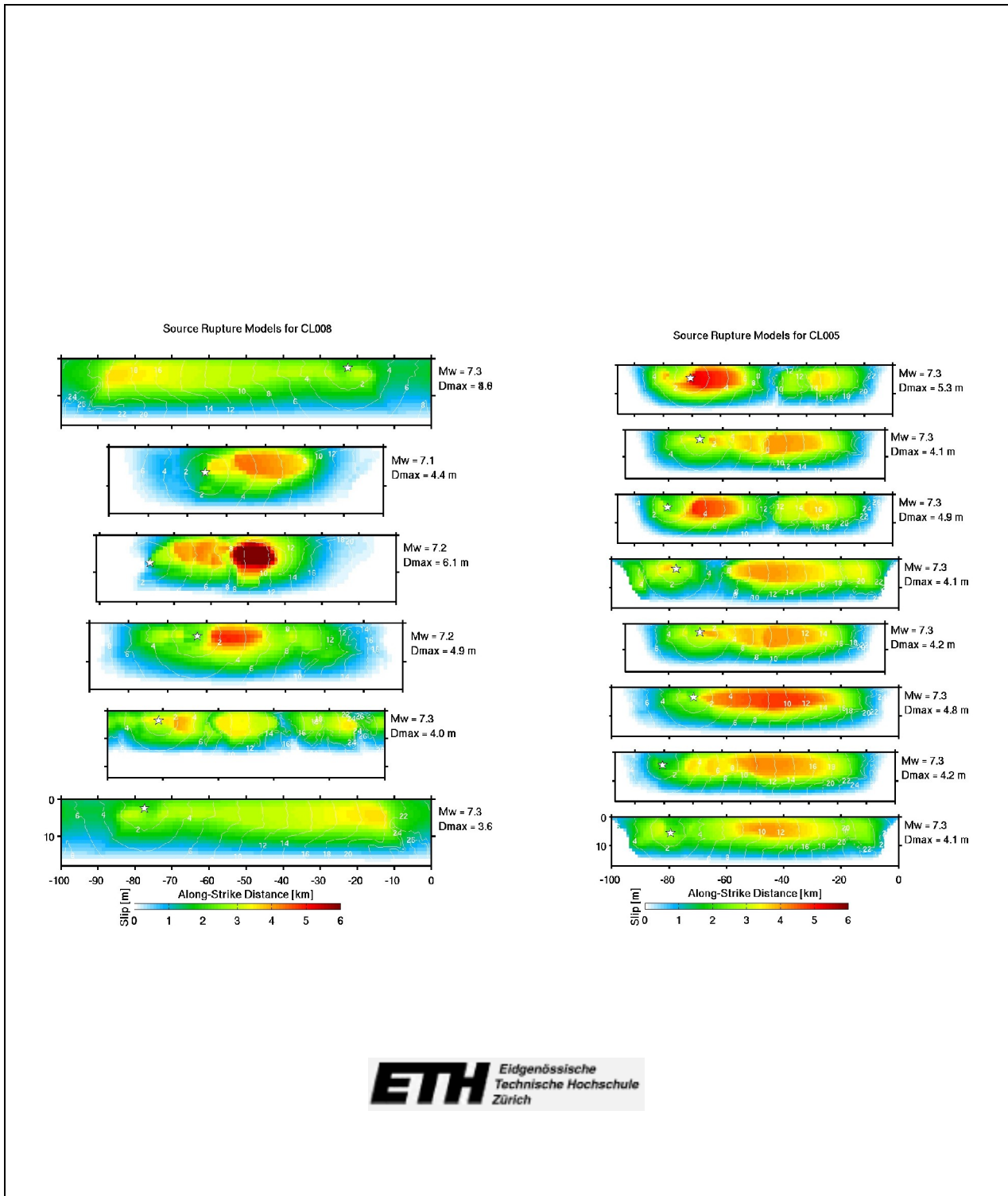


**Figure 3.3** Pseudo-dynamic source models for two classes of friction-parameterizations in the multi-cycle simulations. The star denotes the hypocenter, slip values on the fault plane are color-coded. The rupture time distribution (thin white contours) is calculated using the pseudo-dynamic source characterization (Mai, 2001; Gatterer et al., 2003, 2004).

**Deliverable no. 25 (Partners # 6 and 4: UiB and ETHZ)**



**Project No: EVG1-CT-2002-00069**

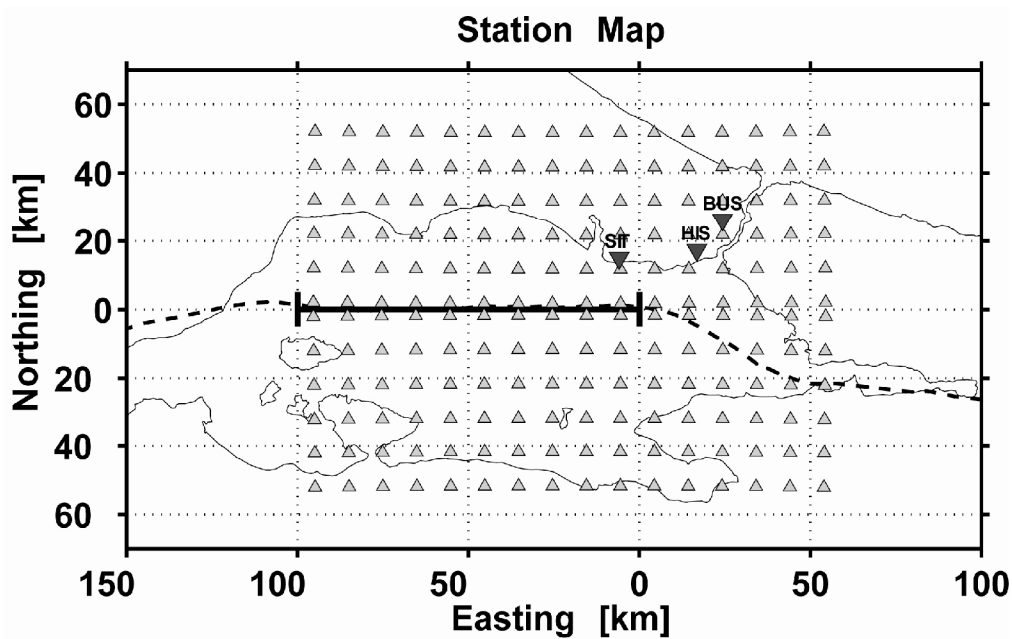


**Figure 3.4** Source-site geometry for ground-motion simulations based on multi-cycle earthquake simulations combined with the pseudo-dynamic source characterization. The broken lines denotes the main strand of the North Anatolian Fault (NAF), the central straight segment (solid line) marks the surface expression of the fault considered for ground motion calculation.

**Deliverable no. 25 (Partners # 6 and 4: UiB and ETHZ)**



**Project No: EVG1-CT-2002-00069**

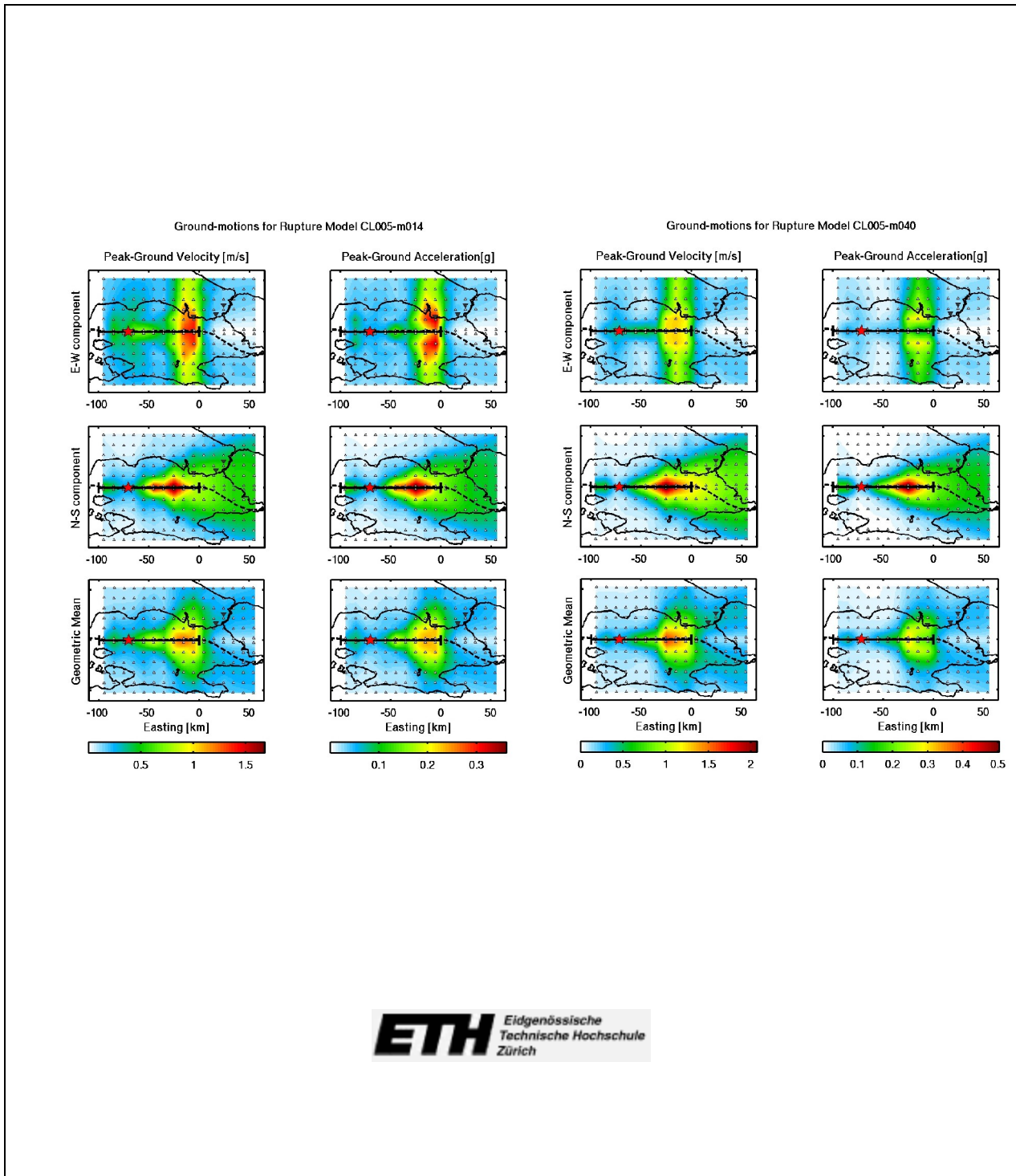


**Figure 3.5** Color-coded spatial distribution of *PGV* (first and third column) and *PGA* (second and fourth column) of the east-west (top), north-south (middle) and geometric-mean component (bottom), computed for two scenario events. The red star marks the hypocenter. Clearly visible are the strong directivity effects for the rupture propagating towards the city of Istanbul.

**Deliverable no. 25 (Partners # 6 and 4: UiB and ETHZ)**



**Project No: EVG1-CT-2002-00069**



## **Appendix I:**

**Revision of the long-term seismicity in the greater Marmara Region  
by N.N. Ambraseys (Sub-contractor's report)**



This document was created with Win2PDF available at <http://www.daneprairie.com>.  
The unregistered version of Win2PDF is for evaluation or non-commercial use only.